Terahertz generation through optical rectification in reflection

Kristensen, Mathias Hedegaard; Herault, Emilie; Zhai, Dongwei; Skovsen, Esben; Coutaz, Jean-Louis

Published in:
Journal of Applied Physics

DOI (link to publication from Publisher):
10.1063/5.0144433

Publication date:
2023

Document Version
Accepted author manuscript, peer reviewed version

Journal of Applied Physics

AIP Publishing

Terahertz generation through optical rectification in reflection

Mathias Hedegaard Kristensen,[1] Emilie Herault,[2] Dongwei Zhai,[2,3] Esben Skovsen,[1] and Jean-Louis Coutaz[2]
[1)]*Department of Materials and Production, Section for Physics and Mechanics, Aalborg University, Skjernvej 4A, DK-9220, Aalborg East, Denmark*
[2)]*IMEP-LAHC, UMR CNRS 5130, Université Savoie Mont Blanc, 73 376 Le Bourget du Lac Cedex, France*
[3)]*College of Physics, Qingdao University, Qingdao 266071, China*

(*Electronic mail: math@mp.aau.dk)

(Dated: 24 March 2023)

In this paper, we study terahertz generation through optical rectification in reflection at normal incidence in a dielectric nonlinear crystal. We first analyse, with a nonlinear optical model, the sample parameters (thickness, absorption at both laser and terahertz wavelengths, etc.) for which a terahertz optical rectification reflection scheme is preferable to the common transmission scheme. Then we report our experimental observations of a reflected terahertz signal generated at the surface of a ZnTe crystal. The reflected terahertz signal shares all the characteristics of a signal generated in transmission, but is not limited by absorption losses in the crystal, thereby providing a broader bandwidth. At high pump laser power, the signal exhibits saturation, which is caused by the decrease of the nonlinear susceptibility due to photocarriers generated by two-photon absorption. This reflection scheme could be of great importance for terahertz microscopy of opaque materials like, e.g., humid samples or samples exhibiting strong absorption bands, or to study samples for which the transmitted signal cannot be recorded.

I. INTRODUCTION

Optical rectification (OR) is an elegant way to produce terahertz (THz) pulses by irradiating a dielectric nonlinear crystal with femtosecond laser pulses. Because of the almost instantaneous polarization of the crystal atoms or molecules, broadband THz pulses may be generated[1]. Moreover, very intense THz peak power can be delivered[2]. Actually, OR corresponds to the difference of frequencies between all the spectral components of the ultra-short laser pulse. In fact, difference-frequency generation was the first opto-electronic technique used to generate far infrared beams[3–5]. Here, difference-frequency generation is named OR because the generated THz frequencies are much smaller than the exciting laser frequency. Usually, generation of THz waves through OR in a crystal is performed in transmission, because the generated THz field magnitude increases linearly with the crystal thickness if phase-matching between the incident laser beam and the generated THz beam is realized. Recently, Sotome *et al.*[6] employed OR in transmission to obtain THz images of ferroelectric samples, where the laser beam was scanned over the sample, and each irradiated point of the sample generated a THz signal whose magnitude was related to both the crystallinity and nonlinearity of the sample. More recently, some of us used the same technique to get THz images of a caster sugar grain with a sub-wavelength resolution[7]. We named this technique Optical Rectification Terahertz Imaging (ORTI). Then, by improving our setup, we published an ORTI image of the domains of a periodically-poled KTP crystal with a lateral resolution of $\lambda/200$.[8] A next progress towards ORTI of actual samples will be to record images in reflection. It will allow one to characterize opaque or bulky samples, or samples whose rear face is rough.

Generation of THz pulses through OR in reflection has only been studied to a lesser extent. In 2005, Reid *et al.*[9] have reported OR THz generation from a semi-conductor recorded in reflection at 45° incidence. They pumped an InAs sample below its bandgap at 800 nm and by a proper polarimetric study of both THz generation and second-harmonic generation (SHG), they were able to discriminate the respective contributions of the bound and free photo-excited electrons. Moreover, they demonstrated the different contributions of both bulk and surface regions of the sample, this difference arising thanks to the surface electric-field. The effect is strong in narrow bandgap semiconductors like InAs, but insignificant in larger bandgap materials, like GaAs. Later in 2007, Zinov'ev *et al.*[10,11] and Bakunov *et al.*[12,13] developed theoretical models of THz generation through OR including a field generated in the backward direction (reflection). Zinov'ev *et al.* presented a thorough description of all the THz pulses generated when an optical pulse propagates through a slab of nonlinear material. Their theoretical calculations clarify that the THz radiation is generated at the surfaces due to the instantaneous creation and acceleration of polarization charge at the front surface, and subsequent deceleration and extinction at the back surface. They supported their theory by experiments measured in transmission. Bakunov *et al.* extended the usual Fresnel formulas for transmission and reflection of free-propagating electromagnetic pulses to forced pulses generated in a nonlinear crystal and showed that the free and forced waves obey different boundary conditions at the crystal surfaces.[12] In the second paper[13], they expanded their model to include the focusing of the pump beam and calculate the Cherenkov angular spreading of the generated THz waves. Later on, Hargreaves *et al.*[14] published a detailed modeling on THz OR generation versus the crystal orientation in view of clearly discriminating OR and photo-induced current transient contributions. Finally, A. Schneider[15] performed a complete analysis of the THz pulses generated in a nonlinear slab considering dispersion, absorption of both optical and terahertz waves, and multiple reflections. Furthermore, OR THz generation in reflection has been performed when dealing with

opaque materials, like metals[16].

In most of these publications, the research was focused on the theoretical description of the OR THz generation. When experimental results were reported, they were performed either in transmission[11,17] or under oblique incidence.[9,16] From a practical point of view when dealing with applications like ORTI, THz OR generation in reflection under normal incidence is preferable. The goal of this paper is not to propose a highly efficient scheme for high power THz generation, but to show that OR in reflection can be used to study the THz response of samples. Moreover, generation in reflection is the only available OR technique when samples are absorbing and too thick, or if their rear face does not allow a good transmission of the THz beam (rough surface, surface covered with opaque films like metallic ones, etc.). Especially, we will 1) evaluate for which samples OR in reflection supplies stronger signals than OR in transmission, and thus should be preferred; 2) experimentally demonstrate THz OR generation in reflection under normal incidence. This study is performed with ZnTe as dielectric nonlinear crystal.

II. MODELING

Let us recall some basic expressions of OR generated THz fields. We will deal only with the case of normal incidence. The laboratory reference frame is (xyz) and the laser beam propagates normally to the crystal surface along the z-direction. We suppose that the irradiating laser beam is a plane wave with two spectral components at ω and $\omega+\Omega$ (ω and Ω are respectively the optical and THz angular frequencies). The plane wave is a good approximation when the laser beam is not strongly focused onto the sample, *i.e.* the laser Rayleigh length is larger than the crystal thickness d. We choose the following notation for the electrical field of this plane wave in air:

$$\vec{E}_{o,\omega}(z,t)=\vec{E}_{o,\omega}(z)\,e^{-j\omega t}=\vec{E}_{o,\omega}\,e^{jk_{o,\omega}z}e^{-j\omega t}. \qquad (1)$$

$\vec{k}_{o,\omega}=\frac{\omega}{c}\vec{u}_z$ is the incident wave vector (c is the velocity of light in vacuum, $\vec{u}_z$ is the unit vector along direction z). We neglect the anisotropy of the crystal. Inside the crystal, the laser field is

$$\vec{E}_{\omega}(z)=\vec{E}_{\omega}\,e^{j\tilde{k}_{\omega}z}=\tilde{t}_{\omega}\vec{E}_{o,\omega}\,e^{j\tilde{k}_{\omega}z}. \qquad (2)$$

with wavevector $\vec{\tilde{k}}_{\omega}=\frac{\omega}{c}\tilde{n}_{\omega}\vec{u}_z$ and transmission coefficient $\tilde{t}_{\omega}$ at the crystal surface (we employ a tilde to indicate complex values except for complex fields). Here, $\tilde{n}_{\omega}=n_{\omega}+j\kappa_{\omega}$ is the complex refractive index of the crystal at the laser frequency. The THz wave at frequency Ω is generated through OR, *i.e.* a second order nonlinear effect. The related nonlinear polarization is

$$\vec{P}_{\Omega}^{\mathrm{NL}}(z)=\varepsilon_o\overset{\leftrightarrow}{\tilde{\chi}}^{(2)}:\vec{E}_{\omega+\Omega}(z)\cdot\vec{E}_{\omega}^{*}(z). \qquad (3)$$

ε_o is the permittivity of vacuum, $\overset{\leftrightarrow}{\tilde{\chi}}^{(2)}$ is the nonlinear OR tensor, and the asterisk denotes the complex conjugate. The nonlinear Helmholtz propagation equation for the THz field $\vec{E}_{\Omega}$ is:

$$\nabla^2\vec{E}_{\Omega}(z)+\frac{\Omega^2}{c^2}\tilde{\varepsilon}_{\Omega}\vec{E}_{\Omega}(z)=-\frac{\Omega^2}{c^2}\overset{\leftrightarrow}{\tilde{\chi}}^{(2)}:\vec{E}_{\omega+\Omega}(z)\cdot\vec{E}_{\omega}^{*}(z). \qquad (4)$$

In order to derive the THz fields reflected and transmitted outside the crystal, we neglect the rebounds of the laser and THz pulses inside the crystal. We then substitute the laser field in Eq. (4) with the expression from Eq. (2), and thus, the nonlinear term writes:

$$\overset{\leftrightarrow}{\tilde{\chi}}^{(2)}:\vec{E}_{\omega+\Omega}(z)\cdot\vec{E}_{\omega}^{*}(z)=\overset{\leftrightarrow}{\tilde{\chi}}^{(2)}:\vec{E}_{\omega+\Omega}\cdot\vec{E}_{\omega}e^{j\left(\tilde{k}_{\omega+\Omega}-\tilde{k}_{\omega}^{*}\right)z}. \qquad (5)$$

The wave vector difference

$$\begin{aligned}\tilde{k}_{\omega+\Omega}-\tilde{k}_{\omega}^{*}=&\frac{\omega+\Omega}{c}n_{\omega+\Omega}-\frac{\omega}{c}n_{\omega}\\&+j\frac{\omega}{c}\left(\left(1+\frac{\Omega}{\omega}\right)\kappa_{\omega+\Omega}+\kappa_{\omega}\right)\end{aligned} \qquad (6)$$

simplifies as

$$\Delta\tilde{k}=\tilde{k}_{\omega+\Omega}-\tilde{k}_{\omega}^{*}\approx\frac{\Omega}{c}n_{\mathrm{G},\omega}+j\alpha_{\omega}\equiv\frac{\Omega}{c}\tilde{n}_{\mathrm{G},\omega}, \qquad (7)$$

assuming $\Omega\ll\omega$ and using the group index $n_{\mathrm{G},\omega}=n_{\omega}+\omega\frac{\partial n_{\omega}}{\partial\omega}$. In Eq. (7), $\alpha_{\omega}=\frac{2\omega}{c}\kappa_{\omega}$ is the coefficient of absorption at the laser wavelength. It follows that

$$\tilde{n}_{\mathrm{G},\omega}\equiv n_{\mathrm{G},\omega}+j\frac{c}{2\omega}\alpha_{\mathrm{G},\omega}\quad\Rightarrow\quad\alpha_{\mathrm{G},\omega}=\frac{2\omega}{\Omega}\alpha_{\omega}. \qquad (8)$$

Solving the boundary equations at the surface ($z=0$) within this hypothesis, the reflected THz field is given by

$$\vec{E}_{\mathrm{R},\Omega}(z)=-\frac{\overset{\leftrightarrow}{\tilde{\chi}}^{(2)}:\vec{E}_{\omega+\Omega}\cdot\vec{E}_{\omega}^{*}}{(\tilde{n}_{\Omega}+1)(\tilde{n}_{\mathrm{G},\omega}+\tilde{n}_{\Omega})}e^{-jk_{\mathrm{R},\Omega}z}. \qquad (9)$$

$\tilde{n}_{\Omega}$ is the refractive index at the THz frequency, and $k_{\mathrm{R},\Omega}=\Omega/c$. When dealing with ultrashort laser pulses, expression (9) must be integrated over the whole laser pulse spectrum (see for example eqs. (7) and (20) in the paper by Schneider *et al.*[17]). This is compulsory when one desires to determine the upper spectral limit of the generated THz signal, or to fit the experimental spectra. Let us notice that in Eq. (9)

$$\tilde{n}_{\mathrm{G},\omega}+\tilde{n}_{\Omega}=n_{\mathrm{G},\omega}+n_{\Omega}+j\frac{c}{2\Omega}(2\alpha_{\omega}+\alpha_{\Omega}), \qquad (10)$$

which is deduced from Eq. (7). As expected, the reflected field does not depend on the crystal thickness and exists even if the crystal thickness tends towards zero: The generation in reflection is a pure surface effect. The reflected field magnitude depends on the crystal nonlinearity and only slowly on the crystal refractive index. Therefore the reflected THz signal exhibits all the spectral features related to the linear and nonlinear properties of the crystal at both laser and THz frequencies. Especially, phonon resonances at THz frequencies should be clearly observed in the reflected THz spectrum. Fig. 1(a) shows the magnitude normalized to the nonlinear source, *i.e.*

$$\left|\vec{E}_{\mathrm{R},\Omega}/\overset{\leftrightarrow}{\tilde{\chi}}^{(2)}:\vec{E}_{\omega+\Omega}\cdot\vec{E}_{\omega}^{*}\right|=\left|(\tilde{n}_{\Omega}+1)(\tilde{n}_{\mathrm{G},\omega}+\tilde{n}_{\Omega})\right|^{-1},$$

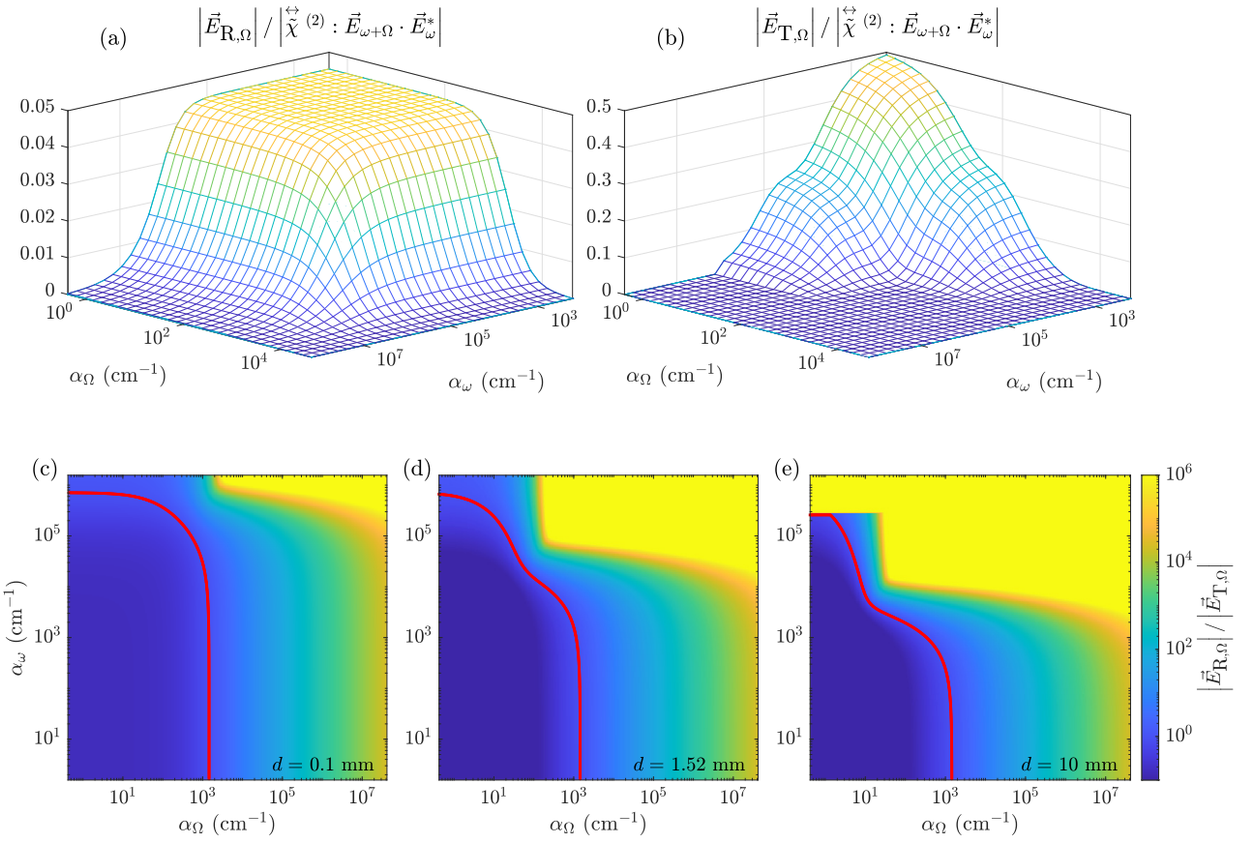

FIG. 1. Maps of the THz field magnitudes generated in reflection (a) and transmission (b) normalized to the nonlinear source using $\lambda = 2\pi c/\omega = 800$ nm, $f = 1$ THz, $n_{\mathrm{G},\omega} = 2.5$, $n_\Omega = 3$, and $d = 1.52$ mm, versus the optical and THz absorption coefficients. The contour map of the ratio (Eq. (13)) is plotted in the case of phase-matching ($n_{\mathrm{G},\omega} = n_\Omega = 3$) for $d = 0.1$ mm (c), $d = 1.52$ mm (d) and $d = 10$ mm (e). The red lines indicate the unity ratio.

for $\lambda = 2\pi c/\omega = 800$ nm, $f = 1$ THz, $n_{\mathrm{G},\omega} = 2.5$ and $n_\Omega = 3$ versus the absorption coefficients $\alpha_{\mathrm{G},\omega}$ and α_Ω. We see that the reflected field magnitude is almost constant up to $\alpha_\omega \approx 10^6$ cm^{-1} and $\alpha_\Omega \approx 10^3$ cm^{-1} (the yellow plateau), whereupon it decreases strongly and becomes zero. We can conclude that for most of materials, even if they exhibit a rather large absorption at both laser and THz wavelengths, the reflected THz field does not depend so much on the loss. It vanishes only for materials that are practically opaque.

Let us now treat the transmitted THz field. At a distance z inside the crystal, the field is the sum of the propagating free and forced waves:

$$\vec{E}_\Omega(z) = \frac{\overleftrightarrow{\tilde{\chi}}^{(2)} : \vec{E}_{\omega+\Omega} \cdot \vec{E}_{\omega}^{*}}{\tilde{n}_{\mathrm{G},\omega}^2 - \tilde{n}_\Omega^2} \left(e^{j\Delta\tilde{k}z} - \frac{\tilde{n}_{\mathrm{G},\omega}+1}{\tilde{n}_\Omega+1} e^{j\tilde{k}_\Omega z} \right) \quad (11)$$

with $\tilde{k}_\Omega = \frac{\Omega}{c}\tilde{n}_\Omega$. The field transmitted at the exit face of the crystal ($z > d$) must be multiplied by the THz transmission coefficient $\tilde{t}_\Omega$:

$$\vec{E}_{\mathrm{T},\Omega}(z) = \vec{E}_\Omega(d)\,\tilde{t}_\Omega e^{jk_{\mathrm{R},\Omega}(z-d)}. \quad (12)$$

The magnitude of the transmitted field normalized to the nonlinear source,

$$\left|\vec{E}_{\mathrm{T},\Omega} / \overleftrightarrow{\tilde{\chi}}^{(2)} : \vec{E}_{\omega+\Omega} \cdot \vec{E}_{\omega}^{*}\right| = \left| \frac{2\tilde{n}_\Omega}{1+\tilde{n}_\Omega} \frac{2\left(e^{j\Delta\tilde{k}d} - \frac{\tilde{n}_{\mathrm{G},\omega}+1}{\tilde{n}_\Omega+1} e^{j\tilde{k}_\Omega d} \right)}{(\tilde{n}_\Omega+1)\left(\tilde{n}_{\mathrm{G},\omega}^2 - \tilde{n}_\Omega^2\right)} \right|,$$

is plotted in Fig. 1(b) using similar parameter values as for the reflected field and crystal thickness $d = 1.52$ mm (this is the thickness of the sample studied in the experimental part. It corresponds to a typical value for a rather efficient and broadband THz OR generation in transmission). The transmitted THz signal decreases strongly when the visible and/or THz absorption increase. Typically, it is almost null when $\alpha_\Omega > 10^3$ cm^{-1} or $\alpha_\omega > 10^7$ cm^{-1}. Finally, let us compare the magnitudes of the reflected and transmitted THz fields:

$$\left|\frac{\vec{E}_{\mathrm{R},\Omega}}{\vec{E}_{\mathrm{T},\Omega}}\right| = \left| \frac{(\tilde{n}_\Omega+1)(\tilde{n}_{\mathrm{G},\omega}-\tilde{n}_\Omega)}{4\tilde{n}_\Omega\left(e^{j\Delta\tilde{k}d} - \frac{\tilde{n}_{\mathrm{G},\omega}+1}{\tilde{n}_\Omega+1} e^{j\tilde{k}_\Omega d} \right)} \right|. \quad (13)$$

The ratio is independent on the crystal nonlinearity, and thus, on the polarization of the laser and THz beams. For weak visible and THz absorption, the transmitted THz signal is much stronger than the reflected signal due to cumulative generation

throughout the crystal. At higher absorption, laser and/or THz beams no longer propagate inside the crystal. This appears clearly on the contour maps plotted in Fig. 1(c) for $d = 0.1$ mm, Fig. 1(d) for $d = 1.52$ mm, and Fig. 1(e) for $d = 1$ cm. The red line represents the unity ratio. For the $d = 1.52$ mm sample, the red line limit occurs at $\alpha_\Omega \approx 10^3$ cm^{-1} for crystals with an absorption α_ω at the laser frequency less than $\sim 10^3$ cm^{-1}. For large absorption values at the laser frequency, the reflected signal is of course stronger than the transmitted one at an absorption weaker than for thinner samples. In conclusion, for most of the common materials with standard thicknesses, THz generation by OR in transmission is more efficient than in reflection, and hence, the reflection technique is practically useful only if the sample or the experimental geometry does not allow to measure the transmitted signal. This is the case for samples whose exit face is rough or covered by a metallic film. For absorption values beyond this red contour, *i.e.* for materials like water[18] or carbon-fiber composites[19] ($\alpha_\Omega \sim 1000$ cm^{-1}), the reflected signal is stronger than the transmitted signal. However, we must keep in mind that its magnitude is very weak, even if stronger than the transmitted one. The difference between the reflected and transmitted signals is emphasized when plotting the field magnitudes versus the difference $n_{G,\omega} - n_\Omega$. Fig. 2(a) shows the transmitted and reflected THz fields versus $n_{G,\omega} - n_\Omega$ for $n_{G,\omega} = 3$ and $f = 1$ THz. We assume that the crystal is $d = 1.52$ mm thick and transparent at the laser wavelength ($\lambda = 800$ nm). The transmitted field is plotted for different values of the THz absorption. Because the reflected field depends weakly on the THz absorption, we plot it only for $\alpha_\Omega = 0$ cm^{-1}. The phase-matching oscillations in transmission are clearly seen when the THz absorption is null, while the much weaker reflection curve does not show any phase-matching feature. Typically, at 1 THz with $n_\Omega = 3.2$, $n_{G,\omega} = 3.16$ and $d = 1.52$ mm, one obtains $E_R/E_T = 1/90$. With increasing THz absorption, the transmitted THz signal decreases and its oscillations are attenuated. However, when the sample is almost opaque to THz waves ($\alpha_\Omega = 1000$ cm^{-1}, like water[18] or carbon-fiber composites[19]), the phase-matching maximum is erased and the transmitted field is comparable to the reflected field. Fig. 2(b) presents similar curves, but calculated for a given THz absorption ($\alpha_\Omega = 20$ cm^{-1}) and different crystal thicknesses. Because of the phase-matching phenomenon, the transmitted curves show oscillations whose pseudo-periodicity is shorter with thinner crystals. Here the effect of THz absorption is compensated by increasing the crystal thickness when phase-matching is realized. Thus, as before (Fig. 2(a)), the transmitted field is stronger than the reflected one by 1-2 orders of magnitude when phase-matching is realised.

Hence, it appears that, even for transparent crystals and without achieving phase-matching, the signal generated in reflection is much smaller than the one in transmission. Therefore, OR performed in reflection is not a technique that produces high power THz pulses. It should be used when studying materials that are opaque or scatter in the THz range, or whose rear face is rough, or covered by nontransparent or diffracting layers. Also, it could be of interest when a reflection scheme is easier to implement than a transmission one, for example in microscopy. In all other cases, a transmission arrangement is more efficient.

Let us now address the error on the transmitted THz field made when the reflected THz is omitted. Instead of expression (11), one gets:

$$\vec{E}_\Omega^{\text{approx}}(d) = \frac{\overleftrightarrow{\tilde{\chi}}^{(2)} : \vec{E}_{\omega+\Omega} \cdot \vec{E}_\omega^*}{\tilde{n}_{G,\omega}^2 - \tilde{n}_\Omega^2} \left(e^{j\Delta\tilde{k}d} - e^{j\tilde{k}_\Omega d} \right). \tag{14}$$

The relative error writes:

$$\frac{\vec{E}_\Omega^{\text{approx}}(d) - \vec{E}_\Omega(d)}{\vec{E}_\Omega(d)} = \frac{\tilde{n}_{G,\omega} - \tilde{n}_\Omega}{(1+\tilde{n}_\Omega)\, e^{j(\Delta\tilde{k}-\tilde{k}_\Omega)d} - 1 - \tilde{n}_{G,\omega}}. \tag{15}$$

Typically, this error is almost constant with $\tilde{n}_\Omega - \tilde{n}_{G,\omega}$, but it depends strongly on the crystal thickness d. For a transparent crystal, and at 1 THz, the error is much less than 1 % for d larger than 1 mm, and thus, it could be neglected. But it increases to $\sim 7\%$ for $d = 100$ μm and up to $\sim 30\%$ for $d = 10$ μm. In such very thin crystals, used to generate very broadband THz signals,[20] generation in transmission is weak because the crystal thickness is small. Thus, the amplitudes of the reflected and transmitted THz signals become of the same order of magnitude. Therefore, the reflected field can no longer be omitted.

The generated THz fields depend on the nonlinear source term $\overleftrightarrow{\tilde{\chi}}^{(2)} : \vec{E}_{\omega+\Omega} \cdot \vec{E}_\omega^*$. This nonlinear term has to be calculated in the crystal frame (XYZ), in which the nonlinear tensor $\overleftrightarrow{\tilde{\chi}}^{(2)}$ is known. To switch from the laboratory to the crystal frame, a first rotation by θ around y is performed followed by a second rotation by ϕ around z.[21] The whole rotation matrix R is:

$$R(\phi,\theta) = \begin{pmatrix} \cos\phi\cos\theta & -\sin\theta & \cos\phi\sin\theta \\ \sin\phi\cos\theta & \cos\theta & \sin\phi\sin\theta \\ -\sin\theta & 0 & \cos\theta \end{pmatrix}. \tag{16}$$

The nonlinear polarization $\vec{P}_{\Omega,XYZ}^{\text{NL}}$ in Eq. (4) is calculated in the crystal frame using

$$\vec{E}_{\omega,XYZ} = R(\phi,\theta)\, \vec{E}_{\omega,xyz}$$

and then multiplied by the inverse rotation matrix $R^{-1}(\phi,\theta)$ to obtain the expression in the laboratory frame:

$$\begin{aligned} \vec{P}_{\Omega,xyz}^{\text{NL}} =& R^{-1}(\phi,\theta)\, \varepsilon_o \\ & \times \overleftrightarrow{\tilde{\chi}}^{(2)} : \left(R(\phi,\theta)\, \vec{E}_{\omega+\Omega,xyz} \right) \cdot \left(R(\phi,\theta)\, \vec{E}_{\omega,xyz}^* \right). \end{aligned} \tag{17}$$

Expression (17) must be calculated for each crystallographic class and each orientation of the crystal. In the case of cubic crystals (432, $\bar{4}3m$, 23) addressed here, the nonlinear susceptibility tensor is:

$$\overleftrightarrow{\tilde{\chi}}^{(2)} = \begin{pmatrix} 0 & 0 & 0 & \tilde{\chi}_{14}^{(2)} & 0 & 0 \\ 0 & 0 & 0 & 0 & \tilde{\chi}_{14}^{(2)} & 0 \\ 0 & 0 & 0 & 0 & 0 & \tilde{\chi}_{14}^{(2)} \end{pmatrix}. \tag{18}$$

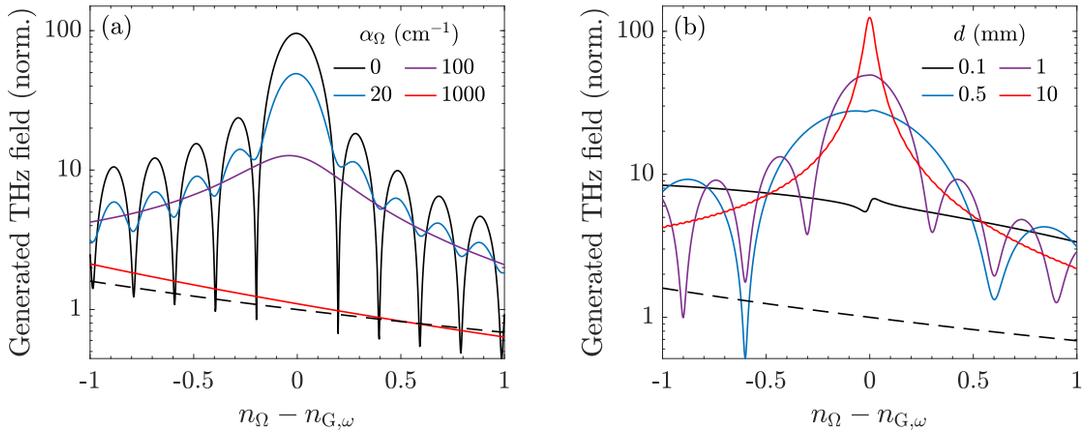

FIG. 2. Calculated transmitted (continuous lines) and reflected (dashed line) THz field magnitudes versus $n_{G,\omega} - n_\Omega$. All the curves are normalized to the reflected signal at $n_{G,\omega} - n_\Omega = 0$. (a) The sample ($d = 1.52$ mm) is assumed to be transparent at the laser wavelength and $n_{G,\omega} = 3$. (b) The THz absorption is assumed to be $\alpha_\Omega = 20$ cm^{-1} and the curves are calculated for different crystal thicknesses, namely $d = 0.1$, 0.5, 1 and 10 mm.

For the most common crystal cuts $\langle 110 \rangle$ and $\langle 111 \rangle$, the rotation angles are respectively

$$\theta = \frac{\pi}{2}, \phi = \frac{\pi}{4} \quad \text{and} \quad \theta = \arccos\left(\frac{1}{\sqrt{3}}\right), \phi = \frac{\pi}{4},$$

which leads to the following dependence of the THz field on the laser polarization angle ψ:[21]

$$\langle 110 \rangle \quad \rightarrow \quad \vec{E}_{R,\Omega}, \vec{E}_{T,\Omega} \propto \frac{1}{4} \begin{pmatrix} \cos 2\psi - 1 \\ -2 \sin 2\psi \\ 0 \end{pmatrix} \tag{19}$$

$$\langle 111 \rangle \quad \rightarrow \quad \vec{E}_{R,\Omega}, \vec{E}_{T,\Omega} \propto \frac{1}{\sqrt{6}} \begin{pmatrix} \cos 2\psi \\ -\sin 2\psi \\ -1/\sqrt{2} \end{pmatrix} \tag{20}$$

Here, we model the THz OR generation in the framework of plane waves interaction. However, if strongly focusing the exciting laser beam in view of performing ORTI microscopy, the issue of focusing the pump laser beam is of utmost importance. Such an issue is very difficult to address, as both laser and THz beams encounter diffraction, and the nonlinear process in the crystal is made complicated because each spatial plane wave component of the incident laser beam exhibits a E-field polarized in a slightly different direction. A complete modeling taking into account the finite size of the exciting laser beam has already been treated by Bakunov *et al.*[13]: When the laser beam is not strongly focused, the generated THz beam is very similar to a one-dimensional beam (plane wave-like of limited radial size). On the other hand, when the laser spot size at the crystal entrance is smaller than the involved THz wavelengths, a Cherenkov cone is generated inside the crystal and both the transmitted and reflected THz beam are highly diverging outside the crystal: The excited area of the crystal behaves almost as a THz point-source. In the hypothesis of a crystal thickness that is smaller than the laser beam Rayleigh length, Schneider *et al.*[17] came to the same conclusion and gave a simple analytical expression of the generated THz beam, assuming the realization of phase-matching and no absorption at both laser and THz frequencies. THz generation by optical rectification in transmission, with a sub-wavelength Gaussian-shaped spot source, has been modeled and measured by H. Lin and coworkers[22]. When the laser spot size is much smaller than the THz wavelength, the THz beam is diffracted in nearly all directions from the crystal independently of the frequency, and it obeys the obliquity factor law. The main result is a decrease of the signal collected by an aperture-limited receiving system. Oppositely, for large laser spot size, the generated THz beam is almost a paraxial Gaussian-like beam. For intermediate laser spot size, the diffraction effect is more pronounced for the lower frequency range, making the corresponding signal detected with a weaker efficiency than the high frequency range. Here, a similar behavior is expected, as only the excited spot at the sample surface radiates the THz field. In the case of ORTI microscopy, as-large-as-possible aperture optics must be employed in front of the receiver in order to collect the maximum of all the THz reflected light spread in a 2π solid angle. Let us point out that, even in the case of strong focusing, all the spectral features of the THz field will be saved.

III. EXPERIMENT

The experimental setup used for THz generation through OR in reflection (Fig. 3) resembled a THz time-domain spectroscopy setup. A beam of 100-fs linearly polarized laser pulses at 80 MHz repetition rate was delivered by a Ti:sapphire oscillator (Spectra-Physics Tsunami, 786 nm center wavelength, and 12.5 nJ pulse energy). A beam splitter

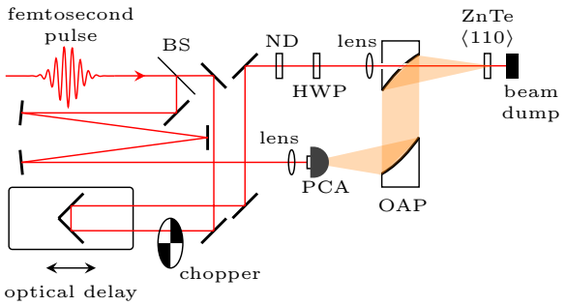

FIG. 3. Illustration of the experimental setup. ND, variable neutral density filter. BS, beam splitter; HWP, half-wave plate; PCA, photoconductive antenna; OAP, off-axis parabolic mirror.

(BS) divided the pulses into a pump and a probe branch. A half-wave plate (HWP) and a mechanical chopper in the pump beam controlled the pump polarization and triggered the lock-in detection, respectively. The pump beam was focused by a 150-mm focal lens on a 1.52-mm thick ⟨110⟩-cut ZnTe crystal at normal incidence through a hole in an off-axis parabolic mirror (OAP). At the crystal, the spotsize diameter was 37 μm and the maximum average laser power was approximately 400 mW without the chopper. A neutral density filter (ND) was used to control the laser power at the crystal. The reflected THz radiation generated through OR was collected by the same parabolic mirror and focused onto a photoconductive antenna (PCA) by a second OAP. The bow-tie PCA detector (BATOP GmbH) was oriented such that it was sensitive to vertically polarized THz radiation. Finally, the measurements were done under ambient conditions.

IV. RESULTS AND DISCUSSION

Fig. 4(a) shows two THz pulses separated by $\Delta t \approx 32.8$ ps (main-peak-to-main-peak). The first THz waveform R was generated through OR in reflection, while the later waveform T was generated in transmission and then reflected at the exit surface of the crystal. The time delay Δt between the two THz waveforms is thus equal to $\Delta t = 2dn_{G,\Omega}/c \approx 2dn_{\Omega}/c$. With the crystal thickness $d = 1.52$ mm and $n_{\Omega} = 3.20$ measured around 1 THz, we get $\Delta t = 32.4$ ps. Let us examine the magnitudes of the R and T pulses. Here, the T pulse is not measured in transmission but is reflected by the exit face of the crystal towards the detector. The great advantage of this scheme over the common transmission one is that both the R and T pulses are excited by the same laser pulse and are measured by the same detector and the same receiving electronics. Therefore, any error due to a difference in sensitivity of a double separated detection (one in reflection and one in transmission) is avoided. Moreover, we took a great care in the alignment of the sample in the THz beam, in such a way the T pulse is directed exactly in the same direction as the reflected one. Laser beams reflected at the entrance and exit faces of the crystal were adjusted to superimpose at the detection system, within a precision better than the laser beam size, *i.e.* less than 1 mm at a 30-cm distance from the crystal. The angular precision is thus better than 0.003 rad = 11 arc min. Let us notice that, generally, crystals are supplied with a parallelism of a few arc min. The ratio of the R and T pulse can be calculated using Eq. (13). However, the transmitted THz field must be multiplied by $\tilde{r}_{\Omega}e^{-\alpha_{\Omega}d/2}$ to include the back reflection at the second crystal surface and transmission through the crystal. With $\alpha_{\Omega} \approx 0$, we get $\left|E_{R,\Omega}/E_{T,\Omega}\right|_{calc} \approx 1/47$. In the recorded trace, we unexpectedly find that the THz peak-to-peak magnitude of waveform R is 7 times stronger compared to waveform T. A possible explanation of the weak T pulse is THz absorption by free carriers generated through a two-photon absorption (TPA) process. Bose *et al.*[23] measured the photogenerated carrier lifetime of ZnTe to be $\tau_{ZnTe} = 25$ ns. The pulse period of the Ti:sapphire oscillator is 12.5 ns. Thus, TPA could lead to a steady state free carrier population that may decrease the THz generation through the crystal, and in turn, absorb the THz radiation reflected at the exit surface. Using the TPA coefficient $\beta \approx 5$ cm/GW [24], $\tau_{ZnTe} \approx 25$ ns, and the Drude model to determine the THz absorption by the mean density of photogenerated carriers, we obtain $\alpha_{\Omega} \approx 80$ cm^{-1}. Contrary, if we extract the absorption coefficient from the measurement using the modified expression (13), we get $\alpha_{\Omega} \approx 77$ cm^{-1} in good agreement with the estimate. As expected, the measured absorption coefficient is slightly lower compared to our estimate, since we do not consider the change of THz transmission/reflection due to the increase of THz absorption.

The THz spectra of waveform R (black) and waveform T (blue) are plotted in Fig. 4(b). The R spectrum is rather smooth (excluding water vapour absorption lines), while the T spectrum exhibits the known sinc function shape with a first zero around 1.5 THz ($f_{cut-off} = c/\pi d(n_{\Omega} - n_{G,\omega}) \approx 1.57$ THz) and two plateaus at 0.9 and 2 THz. The T spectrum is evidently narrower than the R spectrum due to non-perfect phase-matching and exhibits a poor signal-to-noise ratio because its intensity is degraded by linear and TPA absorption when propagating backwards in the crystal. Previously, we hypothesized that the T pulse corresponds to a THz pulse generated in transmission and reflected at the exit face of the crystal. Within this hypothesis, the T spectrum is equal to the R spectrum multiplied by the calculated ratio $\left|E_{T,\Omega}/E_{R,\Omega}\right|$ and by $\tilde{r}_{\Omega}e^{-\alpha_{\Omega}d/2}$ to include the reflection and absorption through the sample. The TPA-induced THz absorption is calculated using a Drude model with the free carrier density as the only adjustable variable. We assume that the crystal is transparent in the visible range. This allows us to get rid of the spectral response of our setup. The calculated spectrum is plotted as a red curve in Fig. 4(b). We see that it corresponds nicely to the measured T spectrum. The best fit is obtained for a carrier density of 1.19×10^{15} cm^{-3}. The photogenerated carrier density can also be estimated from the laser power used in the measurement. Using the TPA coefficient $\beta \approx 5$ cm/GW and $\tau_{ZnTe} \approx 25$ ns, we get a carrier density of 6.49×10^{15} cm^{-3}. This is in fairly good agreement with the above fit as we neglect the TPA effect in the nonlinear propagation equation, which would lead to a higher value of the carrier density calculated from the T spectrum fit. The recorded R spectrum

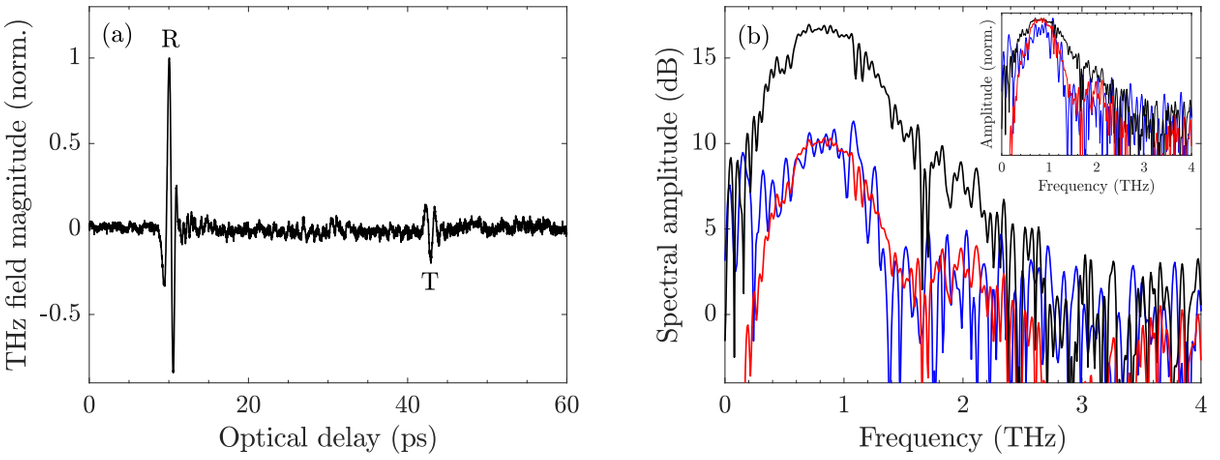

FIG. 4. (a) Waveforms of THz pulses R and T generated through OR in reflection and in transmission, respectively. (b) THz spectra of waveform R (black) and T (blue) and the calculated T spectra (red). The inset shows the R and T spectra normalized to their peak value, which points out the narrower T spectrum as compared to the R spectrum (see comments in the text).

spreads up to 2.7 THz, which is the upper limit (-20 dB) of the Batop bow-tie detector bandwidth. As the reflected pulse is weakly affected by absorption in the crystal, one may expect that its actual spectrum is directly proportional to the laser beam spectral width and could reach some tens of THz with sub-100 fs laser pulses. However, because of the weak magnitude of the reflected signal, detection of this latter requires very sensitive receivers that usually exhibit a long response time, like bolometers. This could be overcome by performing an interferometric measurement that will supply the autocorrelation trace of the generated THz pulses.[25]

The efficiency of the THz generation through OR in reflection vs. pump laser fluence is plotted (circles) in Fig. 5(a) together with a linear fit (dotted) and a TPA-induced saturation fit (red). At weak pump laser fluence, the efficiency is linear, while TPA-induced saturation begins at 200 μJ/cm^2 in good agreement with published results on OR in transmission[26]. This saturation effect is explained by the absorption of the THz signal induced by the TPA photogenerated carriers in the sample. A rigorous analysis requires solving coupled propagation equations with the TPA effect. This is a rather tricky task, which is outside the scope of this paper, as the carrier population dynamics is usually treated in the time domain, while propagation equations are solved in the frequency domain (see for example the pump-and-probe THz studies performed by P. Kužel and his coworkers[27,28]). However, a simple evaluation of the order of magnitude of the influence of TPA can be performed as follows. The photocarrier population modifies both the refractive indices $\tilde{n}_\Omega$ and $\tilde{n}_{G,\omega} \propto \tilde{n}_\omega$ at THz and laser frequencies, respectively. Thus, it changes the magnitude of the reflected THz signal, whose expression is given by Eq. (9). The variation of the real part of $\tilde{n}_{G,\omega}$ is due to the Kerr effect, while its imaginary part is modified by TPA. In ZnTe, the value of the TPA absorption coefficient is $\beta = 5$ cm/GW and the Kerr coefficient is $n_2 \approx 5\times10^{-18}$ m^2/W [29]. In the present experiment, the maximum laser intensity is $I_\omega(\max) \approx 5.5$ GW/cm^2, therefore the photoinduced variation of $\tilde{n}_{G,\omega}$ is $\Delta n_\omega \approx 2.5\times10^{-4}$ and $\Delta\kappa_\omega \approx 2\times10^{-4}$. We conclude that the variation of $\tilde{n}_\omega$ is too small to explain the saturation of the reflected THz field. Let us now address the variation of $\tilde{n}_\Omega$. To take into account the influence of the TPA photocarrier population, we use the Drude model:

$$\tilde{\varepsilon}_\Omega = \varepsilon_\infty - \frac{\omega_p^2}{\omega(\omega+j\Gamma)} = (n_\Omega + j\kappa_\Omega)^2, \quad \omega_p^2 = \frac{N_{TPA}\,e^2}{m_{eff}\varepsilon_o}. \quad (21)$$

Here, N_{TPA} is the TPA photocarrier density, m_{eff} the effective mass of the free electrons, Γ the damping angular frequency, and e the charge of electron. As already explained, we do not take into account the dynamics of N_{TPA}, but we simply take an averaged value in time and over the sample thickness. The absorbed laser intensity due to the TPA effect is

$$\Delta I_\omega = I_\omega\left(1 - e^{-\beta I_\omega d}\right). \quad (22)$$

The number of absorbed photons per laser pulse is

$$N_{pulse} = \Delta I_\omega \frac{\tau_{laser}}{\hbar\omega} S \quad (23)$$

with laser pulse duration τ_{laser}, the reduced Planck constant $\hbar$, and laser spot size S. The TPA-induced photocarrier density is given by

$$N_{TPA} = \eta \frac{N_{pulse}}{Sd}. \quad (24)$$

The coefficient η (not calculated here) renders for the dynamics of the photocarrier population (carrier lifetime, diffusion inside the sample…). We performed the calculation using ZnTe parameters determined by Constable and Lewis[30]: $m_{eff} = 0.151\times m_e$, $\varepsilon_\infty = 7.3$ and $\Gamma = 0.3$ THz. The TPA induces both an increase of absorption and a decrease of the refractive index at THz frequencies. However, the effect of

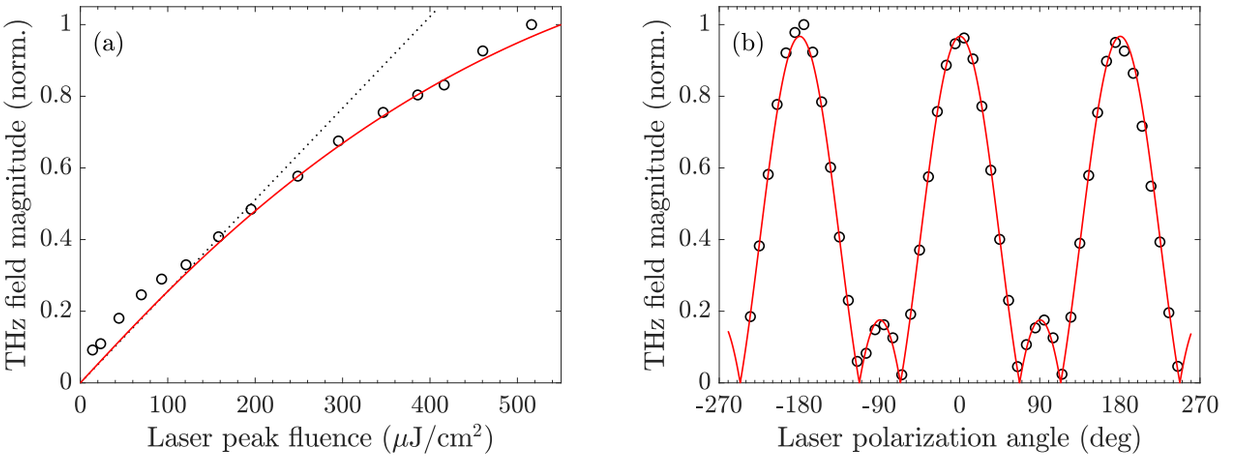

FIG. 5. (a) Measured R pulse amplitude versus laser peak fluence (circles). The dotted straight line is a linear fit while the continuos red curve is calculated taking account TPA as explained in the manuscript. (b) Polarimetric measurements of the R pulse (circles) fitted with the model (red).

the refractive index decrease is stronger in Eq. (9), leading to a small increase of the reflected signal versus the laser intensity. Thus, this can neither explain the observed saturation effect. The only possible reason left for this saturation is the dependence of the nonlinear susceptibility on the carrier density. In a classical model for nonlinear susceptibility[31,32], the magnitude of the nonlinear susceptibility $\overleftrightarrow{\tilde{\chi}}^{(2)}$ is proportional to the magnitudes of the linear susceptibilities at ω and Ω, *i.e.*

$$\begin{aligned}\left|\overleftrightarrow{\tilde{\chi}}^{(2)}\right| &\propto \left|\left(\overleftrightarrow{\tilde{\chi}}^{(1)}_{\omega}\right)^2 \overleftrightarrow{\tilde{\chi}}^{(1)}_{\Omega}\right| \\ &= \left|\left(\tilde{\varepsilon}_\omega - 1\right)^2 \left(\tilde{\varepsilon}_\Omega - 1\right)\right| \\ &= \left|\left(n_\omega + j\kappa_\omega - 1\right)^2 \left(n_\Omega + j\kappa_\Omega - 1\right)\right|.\end{aligned} \tag{25}$$

We calculated the term $\left|\overleftrightarrow{\tilde{\chi}}^{(2)}\right| I_\omega$ of Eq. (9) using the above-described Drude model and the ZnTe parameters by Constable and Lewis[30]. The normalized calculated curve is plotted as a continuous red curve in Fig. 5. We can see the good agreement with our experimental data. The only adjustable parameter is the coefficient η, whose best fitting value is $\eta = 0.259$. This means that just about a quarter of the photoexcited carriers interact with the THz pulse. The reason could be that they both recombine and diffuse inside the sample (Dember effect, both longitudinal and transversal[33,34]) in between two successive laser pulses. Of course, this crude model and the related explanations must be validated by a complete rigorous analysis. Nevertheless, the variation of the nonlinear susceptibility appears to be a prevailing phenomenon when dealing with OR THz generation in a crystal exhibiting a strong TPA effect.

Finally, we perform a polarimetric study of the R pulse. The angle of the linear polarized pump beam $\psi = 2\psi_{\mathrm{HWP}}$ is scanned 360° by adjusting the half-wave plate angle ψ_{HWP} in 5° increments. The bow-tie detector is not strictly sensitive to a single polarization due to its antenna geometry. Therefore, we must fit a weighted expression

$$(1-\gamma)E_{\mathrm{R},\Omega,x} + \gamma E_{\mathrm{R},\Omega,y} \tag{26}$$

of the field components given in Eq. (19) to the data. Additionally, the fit takes into account an angular shift $\delta\psi$ due to disorientation of the crystal axes compared to the laboratory frame. Inspecting Fig. 5(b), we see an excellent agreement of the recorded THz peak magnitude (circles) and our fitted model (red, $\delta\psi = 66.5°$, $\gamma = 0.34$). This value of γ corresponds to a 10% sensitivity of the antenna to the cross polarization, which is within the specifications given by Batop GmbH. Thus, the reflected THz signal contains information of the crystalline orientation of the sample.

V. CONCLUSION

In conclusion, we experimentally demonstrated the generation of a reflected THz signal at normal incidence through OR in a ZnTe crystal. The reflected signal originates in the boundary conditions for the nonlinear fields at the crystal surface. All the characteristics of THz OR generation in the crystal (polarization symmetry, spectral features...) are retrieved in the reflected signal. Its bandwidth is wider than in transmission, because it is not limited by absorption losses in the crystal. At high laser power excitation, the reflected THz signal from ZnTe saturates: It seems that its origin is the effect of TPA, which reduces the magnitude of the second order nonlinear susceptibility. However, for crystals of common mm-thickness that are transparent or exhibit moderate absorption in both the THz and visible domains, the THz reflection magnitude is much smaller than the one in transmission. When dealing with crystals that are opaque in one or both of these spectral domains, or whose rear surface is rough or covered by opaque films like metals, the reflected THz signal is of great interest since the transmitted THz signal is weak or even

zero. This could be applied to THz microscopy of opaque materials, like humid biological samples, e.g. when performing sub-wavelength OR THz imaging[7,8].

ACKNOWLEDGMENTS

We acknowledge fruitful discussions with Prof. F. Laurell and Prof. V. Pasiskevicius, both at the Dept. of Applied Physics, Royal Institute of Technology, Stockholm (Sweden).

REFERENCES

[1] I. Katayama, R. Akai, M. Bito, H. Shimosato, K. Miyamoto, H. Ito, and M. Ashida, "Ultrabroadband terahertz generation using 4-N, N-dimethylamino-4'-N'-methyl-stilbazolium tosylate single crystals," Appl. Phys. Lett. **97**, 021105 (2010).

[2] J. A. Fülöp, Z. Ollmann, C. Lombosi, C. Skrobol, S. Klingebiel, L. Pálfalvi, F. Krausz, S. Karsch, and J. Hebling, "Efficient generation of THz pulses with 0.4 mj energy," Opt. Express **22**, 20155—-20163 (2014).

[3] F. Zernike and P. R. Berman, "Generation of far infrared as a difference frequency," Phys. Rev. Lett. **15**, 999 (1965).

[4] T. Yajima and K. Inoue, "Submillimeter-wave generation by optical difference-frequency mixing of ruby R1 and R2 laser lines," Phys. Lett. A **26**, 281 (1968).

[5] D. W. Faries, K. A. Gehring, P. L. Richards, and Y. R. Shen, "Tunable far-infrared radiation generated from the difference frequency between two ruby lasers," Phys. Rev. **180**, 363 (1969).

[6] M. Sotome, N. Kida, S. Horiuchi, and H. Okamoto, "Visualization of ferroelectric domains in a hydrogen-bonded molecular crystal using emission of terahertz radiation," Appl. Phys. Lett. **105**, 041101 (2014).

[7] F. Sanjuan, G. Gaborit, and J.-L. Coutaz, "Sub-wavelength terahertz imaging through optical rectification," Scientific Reports **8**, 1–7 (2018).

[8] G. Soylu, E. Hérault, B. Boulanger, F. Laurell, and J.-L. Coutaz, "Sub-wavelength THz imaging of the domains in periodically poled crystals through optical rectification," Journal of Infrared, Millimeter, and Terahertz Waves **41**, 1144–1154 (2020).

[9] M. Reid, I. V. Cravetchi, and R. Fedosejevs, "Terahertz radiation and second-harmonic generation from InAs: Bulk versus surface electric-field-induced contributions," Phys. Rev. B **72**, 035201 (2005).

[10] N. N. Zinov'ev, A. S. Nikoghosyan, and J. M. Chamberlain, "Terahertz radiation from a nonlinear slab traversed by an optical pulse," Physical Review Letters **98**, 44801 (2007).

[11] N. N. Zinov'ev, A. S. Nikoghosyan, and J. M. Chamberlain, "Conversion of short optical pulses to terahertz radiation in a nonlinear medium: Experiment and theory," Physical Review B **76**, 235114 (2007).

[12] M. I. Bakunov, A. V. Maslov, and S. B. Bodrov, "Fresnel formulas for the forced electromagnetic pulses and their application fr optical-to-terahertz conversion in nonlinear crystals," Physical Review Letters **99**, 203904 (2007).

[13] M. I. Bakunov, S. B. Bodrov, A. V. Maslov, and M. Hangyo, "Theory of terahertz generation in a slab of electro-optic material using an ultrashort laser pulse focused to a line," Physical Review B **76**, 85346 (2007).

[14] S. Hargreaves, K. Radhanpura, and R. A. Lewis, "Generation of terahertz radiation by bulk and surface optical rectification from crystal planes of arbitrary orientation," Physical Review B **80**, 195323 (2009).

[15] A. Schneider, "Theory of terahertz pulse generation through optical rectification in a nonlinear optical material with a finite size," Physical Review A **82**, 033825 (2010).

[16] F. Kadlec, P. Kužel, and J.-L. Coutaz, "Optical rectification at metal surfaces," Optics Letters **29**, 2674–2676 (2004).

[17] A. Schneider, M. Neis, M. Stillhart, B. Ruiz, R. U. Khan, and P. Günter, "Generation of terahertz pulses through optical rectification in organic DAST crystals: theory and experiment," JOSA B **23**, 1822–1835 (2006).

[18] U. Møller, D. G. Cooke, K. Tanaka, and P. U. Jepsen, "Terahertz reflection spectroscopy of Debye relaxation in polar liquids," JOSA B **26**, A113–A125 (2009).

[19] J. Zhang, C. Shi, Y. Ma, X. Han, W. Li, T. Chang, D. Wei, C. Du, and H.-L. Cui, "Spectroscopic study of terahertz reflection and transmission properties of carbon-fiber-reinforced plastic composites," Optical Engineering **54**, 054106 (2015).

[20] P. Han and X.-C. Zhang, "Coherent, broadband midinfrared terahertz beam sensors," Applied Physics Letters **73**, 3049–3051 (1998).

[21] G. Gaborit, F. Sanjuan, and J.-L. Coutaz, "Second order nonlinear optical processes in [111] cubic crystals for terahertz optoelectronics," Lithuanian Journal of Physics **58** (2018).

[22] H. Lin, C. Fumeaux, B. M. Fischer, and D. Abbott, "Modelling of sub-wavelength thz sources as gaussian apertures," Optics Express **18**, 17672–17683 (2010).

[23] D. Bose, R. Ahrenkiel, and S. Bhunia, "Steady-state and time-resolved photoconductivity measurements of minority carrier lifetime in ZnTe," Journal of Applied Physics **86**, 6599 (1999).

[24] Z.-Y. Zhao, S. Hameau, and J. Tignon, "Thz generation by optical rectification and competition with other nonlinear processes," Chinese Physics Letters **25**, 1868 (2008).

[25] K. Kan, J. Yang, A. Ogata, S. Sakakihara, T. Kondoh, K. Norizawa, I. Nozawa, T. Toigawa, Y. Yoshida, H. Kitahara, *et al.*, "Radially polarized terahertz waves from a photoconductive antenna with microstructures," Applied Physics Letters **102**, 221118 (2013).

[26] F. Sanjuan, G. Gaborit, and J.-L. Coutaz, "Influence of two-photon absorption anisotropy on terahertz emission through optical rectification in zinc-blende crystals," Journal of Infrared, Millimeter, and Terahertz Waves **39**, 378–386 (2018).

[27] H. Němec, F. Kadlec, S. Surendran, P. Kužel, and P. Jungwirth, "Ultrafast far-infrared dynamics probed by terahertz pulses: A frequency domain approach. I. model systems," The Journal of Chemical Physics **122**, 104503 (2005).

[28] H. Němec, F. Kadlec, C. Kadlec, P. Kužel, and P. Jungwirth, "Ultrafast far-infrared dynamics probed by terahertz pulses: A frequency-domain approach. II. applications," The Journal of Chemical Physics **122**, 104504 (2005).

[29] W.-Q. He, C.-M. Gu, and W.-Z. Shen, "Direct evidence of Kerr-like nonlinearity by femtosecond Z-scan technique," Optics Express **14**, 5476–5483 (2006).

[30] E. Constable and R. A. Lewis, "Optical parameters of ZnTe determined using continuous-wave terahertz radiation," Journal of Applied Physics **112**, 063104 (2012).

[31] N. Bloembergen, *Nonlinear Optics* (World Scientific, 1996).

[32] R. W. Boyd, *Nonlinear Optics* (Academic Press, 2020).

[33] V. L. Malevich, R. Adomavičius, and A. Krotkus, "THz emission from semiconductor surfaces," Comptes Rendus Physique **9**, 130–141 (2008).

[34] M. E. Barnes, S. A. Berry, P. Gow, D. McBryde, G. J. Daniell, H. E. Beere, D. A. Ritchie, and V. Apostolopoulos, "Investigation of the role of the lateral photo-dember effect in the generation of terahertz radiation using a metallic mask on a semiconductor," Optics Express **21**, 16263–16272 (2013).

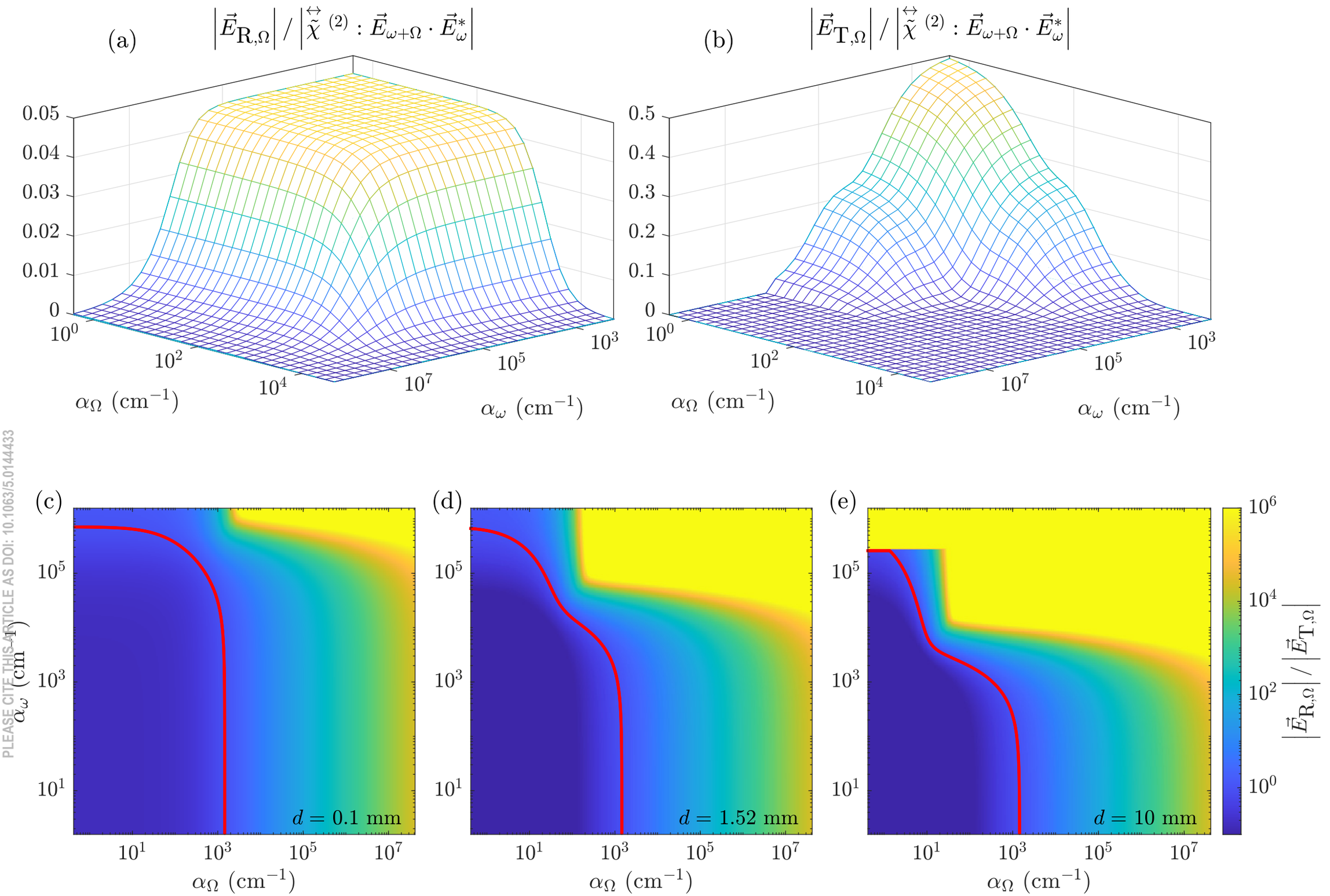

AIP Publishing

Journal of Applied Physics

ACCEPTED MANUSCRIPT

This is the author's peer reviewed, accepted manuscript. However, the online version of record will be different from this version once it has been copyedited and typeset.
PLEASE CITE THIS ARTICLE AS DOI: 10.1063/5.0144433

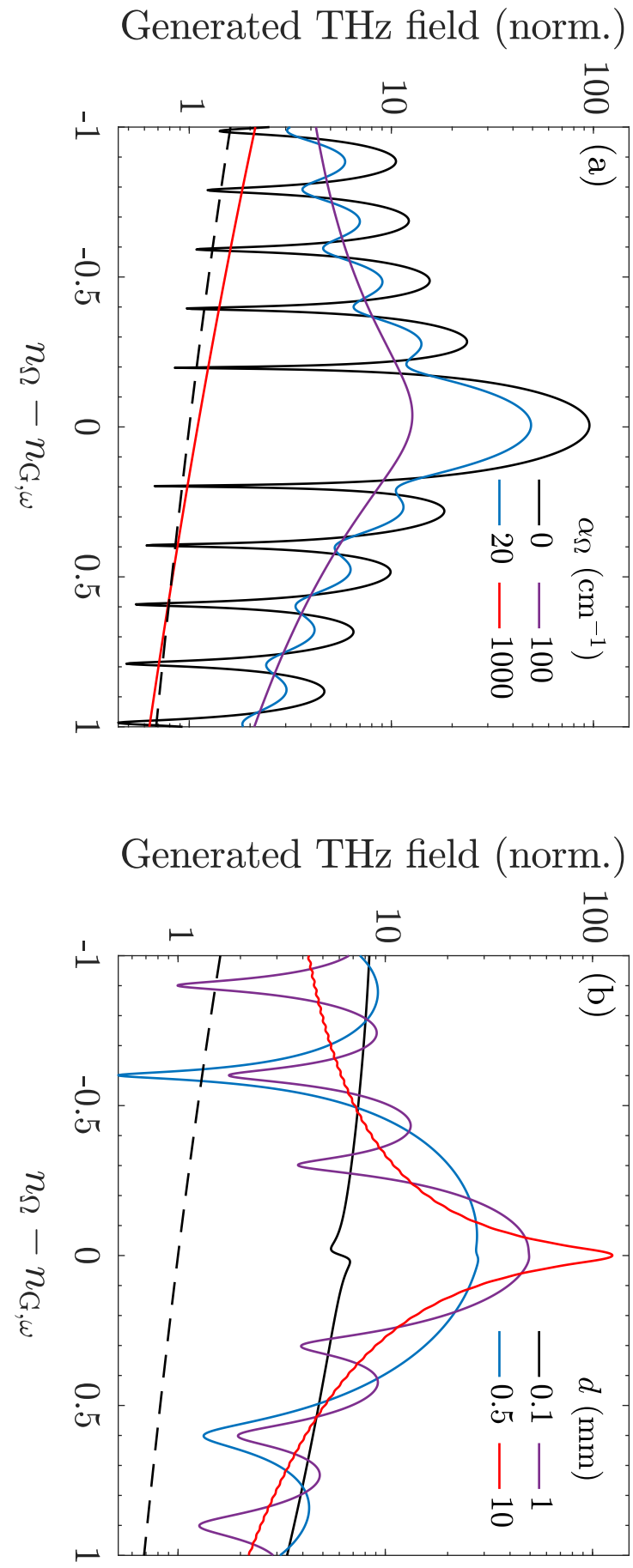

AIP Publishing

Journal of Applied Physics

ACCEPTED MANUSCRIPT

PLEASE CITE THIS ARTICLE AS DOI: 10.1063/5.0144433

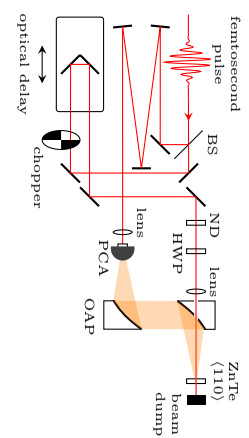

AIP Publishing

Journal of Applied Physics

ACCEPTED MANUSCRIPT

This is the author's peer reviewed, accepted manuscript. However, the online version of record will be different from this version once it has been copyedited and typeset.
PLEASE CITE THIS ARTICLE AS DOI: 10.1063/5.0144433